Theory of electric dipole moments

Yohei Ema,[a,b,*] **Ting Gao**[b] **and Maxim Pospelov**[a,b]

[a] *William I. Fine Theoretical Physics Institute, School of Physics and Astronomy, University of Minnesota,*
Minneapolis, MN 55455, USA

[b] *School of Physics and Astronomy, University of Minnesota,*
Minneapolis, MN 55455, USA

E-mail: ema00001@umn.edu, gao00212@umn.edu, pospelov@umn.edu

I review recent theoretical progress of electric dipole moments (EDMs). After explaining a new Standard Model contribution to paramagnetic EDMs that is recently discovered, I discuss indirect constraints on the muon EDM from the paramagnetic EDM experiments such as ACME.

---

*Speaker

1. Introduction

The EDMs of elementary particles [1–4] represent an important probe of new physics beyond the Standard Model (SM) [5–7]. Recent breakthrough sensitivity to "paramagnetic EDMs" connected to the electron spin [3] established a new limit on the linear combination of the electron EDM d_e and semileptonic CP-odd operators, commonly known as C_S. Given the rapid progress of the last decade, and additional hopes for increased accuracy (see *e.g.* [8–10]), this paper considers two CP violating sources to the paramagnetic EDM experiments; the Standard Model (SM) Cabbibo-Kobayashi-Maskawa (CKM) phase and the muon EDM.

Within the SM, the only source of the CP violation is the phase in the CKM matrix δ_{KM} [11] (apart from the unobserved strong CP phase $\bar{\theta}$), now observed with precision in flavor transitions in B and K mesons. As for the paramagnetic EDM, Ref. [12] recently estimated the size of d_e induced from δ_{KM} (dominated by long-distance effects) as $\sim 6 \times 10^{-40}\, e\,$cm, presumably with considerable hadronic uncertainties. This result is subdominant to the previous C_S estimate coming from the two-photon exchange diagram in combination with $\Delta S = \pm 1$ transitions [13], giving rise to the equivalent d_e of $\sim 10^{-38}\, e\,$cm. The first half of this paper demonstrates that the dominant contribution of δ_{KM} to paramagnetic EDMs is C_S induced by a Kaon-exchange diagram. This has a distinct property in the chiral limit, and is calculable to $\sim 30\%$ accuracy that can be further improved. Remarkably, the resultant equivalent electron EDM is $\sim 10^{-35}\, e\,$cm [14], three orders of magnitude larger than the previous estimate.

We then move our focus on a possible new physcis contribution to the paramagnetic EDM. In particular, we consider the muon EDM as a new source of CP-violation. The muon EDM is a particularly interesting observable given the ongoing discrepancy of the muon $g - 2$ between the theory and experiments [15–17], as these two observables are related as an imaginary and real part of the same operator, respectively. For now, the tightest constraint on the muon EDM comes from the BNL storage ring experiment, $|d_\mu| < 1.8 \times 10^{-19}\, e\,$cm, and this will be significantly improved by the future storage ring experiments [18–22]. On the other hand, the muon EDM generates several other CP-odd operators after integrating out the muon, and those operators are probed with the atomic and molecular EDM experiments [1, 3]. The goal of our second part is to study the indirect constraint on the muon EDM from the atomic and molecular EDM experiments.

2. Standard Model contribution to paramagnetic EDMs

To understand the reach of the EDM experiments to new physics, it is essential to first understand the Standard Model (SM) contribution. Therefore, in this section, we discuss the SM value of the paramagnetic EDM experiments. A paramagnetic atom has an unpaired electron, and is dominantly sensitive to (semi)leptonic CP violations, such as the electron EDM d_e and the semileptonic CP-odd operator C_S, defined as

$$\mathcal{L}_{\mathrm{CPV}} = -\frac{i}{2} d_e \bar{e} \sigma_{\mu\nu} F^{\mu\nu} \gamma_5 e + C_S \frac{G_F}{\sqrt{2}} \left(\bar{e} i \gamma_5 e \right) \bar{N} N, \tag{1}$$

where G_F is the Fermi constant, $F_{\mu\nu}$ is the electromagnetic field strength, e is the electron, and N is the nucleon. It is known that the paramagnetic EDM experiments are sensitive only to a specific
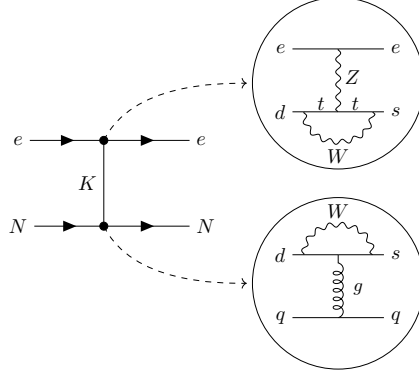
Figure 1: The G_F^3 order diagram that dominates C_S in the chiral limit. The top vertex is the CP-odd, P-even interaction $K_S \bar{e} i \gamma_5 e$ generated at G_F^2 order with one G_F compensated by the top quark mass, and the bottom vertex is the CP-even, P-odd interaction $K_S \bar{N} N$ coupling generated at G_F order.

linear combination of d_e and C_S, which we may define as an *equivalent* electron EDM d_e^{equiv}. The explicit form of the linear combination depends on the specific atomic and/or molecular system, and it is given by

$$d_e^{\text{equiv}} = d_e + C_S \times 1.5 \times 10^{-20} \, e \, \text{cm}, \tag{2}$$

in the case of the ThO molecule. The current best limit is $|d_e^{\text{equiv}}| < 1.1 \times 10^{-29} \, e$ cm [3]. The SM value of d_e is estimated by different groups in the literature. In particular, Ref. [12] recently claims that the long-distance contribution is dominant with its size estimated as $d_e \simeq 6 \times 10^{-40} \, e$ cm. The size of C_S induced by the CKM phase is estimated in the past by [13]. They relied on a two-photon exchange diagram to induce the structure $m_e \bar{e} i \gamma_5 e$, and this contribution scales as $\alpha^2 G_W^2$ with α being the electromagnetic fine structure constant. This contribution is numerically of order $d_e^{\text{equiv}} = O(10^{-38}) \, e$ cm and dominates over the contribution from the electron EDM.

We shall now see that a Kaon-exchange diagram gives a contribution larger by three orders of magnitude than the two-photon exchange one. Although this contribution is formally of order $\alpha_W G_F^3$ with α_W the fine structure constant of the electroweak interaction, one G_F is numerically compensated by the top quark mass as a result of the electroweak penguin diagram. Thus, this contribution is enhanced compared to the previous one by $\alpha_W / \alpha^2 \sim 10^3$

The Kaon-exchange diagram that we consider is shown in Fig. 1. The upper part of the diagram originates from the EW penguin Z-boson exchange/W-box diagram. As we noted above, although EW penguins are formally of order G_F^2, their size is enhanced by the top quark mass, so that the result scales as $G_F^2 m_t^2$. This diagram is theoretically well-established and essential for several flavor-changing processes such as $B_{s,d} \to \mu^+ \mu^-$ and $K_L \to \mu^+ \mu^-$ amplitude. Focusing only on the part relevant to our purpose, the semileptonic operator is concisely written as

$$\mathcal{L}_{\text{EWP}} = -\mathcal{P}_{\text{EW}} \, \bar{e} \gamma_\mu \gamma_5 e \, \bar{s} \gamma^\mu (1 - \gamma_5) d + (h.c.), \quad \mathcal{P}_{\text{EW}} = \frac{G_F}{\sqrt{2}} \times V_{ts}^* V_{td} \times \frac{\alpha_{\text{EM}}(m_Z)}{4\pi \sin^2 \theta_W} I(x_t), \tag{3}$$

where the loop function is given by [23]

$$I(x_t) = \frac{3}{4}\left(\frac{x_t}{x_t - 1}\right)^2 \log x_t + \frac{1}{4}x_t - \frac{3}{4}\frac{x_t}{x_t - 1}, \quad x_t = \frac{m_t^2}{m_W^2}. \tag{4}$$

Below the QCD scale, the quark current $\bar{s}\gamma_\mu(1 - \gamma_5)d$ is matched with the derivatives of the neutral Kaon fields. At the leading order in the chiral perturbation theory, we obtain

$$\mathcal{L}_{Kee} = -2\sqrt{2}f_0 m_e \bar{e}i\gamma_5 e\left(K_S \times \text{Im}\mathcal{P}_{\text{EW}} + K_L \times \text{Re}\mathcal{P}_{\text{EW}}\right), \tag{5}$$

where we used the equation of motion for electrons, where f_0 is the meson decay constant.

We proceed to the lower part of the diagram in Fig. 1, *i.e.*, the $\Delta S = 1$ interaction between the Kaon and the nucleons. Instead of attempting to calculate such a process from first principles (see *e.g.* [24] in this direction), we use the flavor $SU(3)$ relations and connect this coupling to the s-wave amplitudes of non-leptonic hyperon decays [25]. The empirical $\Delta I = 1/2$ rule holds for hyperon decays, and the leading order $SU(3)$ relations fit s-wave amplitudes with $O(10\%)$ accuracy. It is strongly suspected that these amplitudes are indeed induced by strong penguins (SP), but the mechanism behind the $\Delta I = 1/2$ rule is not crucial to us. With that, one can write down the two types of couplings consistent with $(8_L, 1_R)$ transformation properties:

$$\mathcal{L}_{\text{SP}} = -a\text{Tr}(\bar{B}\{\xi^\dagger h\xi, B\}) - b\text{Tr}(\bar{B}[\xi^\dagger h\xi, B]) + (h.c.). \tag{6}$$

where B is the baryon octet matrix, $\xi = \exp[iMf_0^{-1}]$ with M the meson octet matrix, and $h_{ij} = \delta_{i2}\delta_{i3}$ is a spurion that controls the flavor violating structure of the process. Assuming a and b to be real, and taking $f_0 = f_\pi$, they are fit by [25] to be[1]

$$a = 0.56 G_F f_\pi \times [m_{\pi^+}]^2, \quad b = -1.42 G_F f_\pi \times [m_{\pi^+}]^2. \tag{7}$$

The bracket over m_{π^+} represents that this is merely the numerical value $139.5\,\text{MeV}$, and not the theoretical quantity m_π proportional to the quark masses. In the assumption of a and b being real, only the K_S meson couples to nucleons, $2^{1/2}f_0^{-1}((b - a)\bar{p}p + 2b\bar{n}n)K_S$, which will provide the dominant contribution. This type of coupling breaks P but respects CP symmetry. Restoring the CKM factors, one can also include a subdominant coupling to K_L so that we have:

$$\mathcal{L}_{KNN} \simeq -\frac{\sqrt{2}\,G_F \times [m_{\pi^+}]^2 f_\pi}{|V_{ud}V_{us}|f_0} \times 2.84(0.7\bar{p}p + \bar{n}n) \times \left(\text{Re}(V_{ud}^*V_{us})K_S + \text{Im}(V_{ud}^*V_{us})K_L\right). \tag{8}$$

Finally, we integrate out the Kaons in Fig. 1. Adopting it for a nucleus containing $A = Z + N$ nucleons, one arrives at the prediction of C_S induced by the CKM phase:

$$C_S \simeq \mathcal{J} \times \frac{N + 0.7Z}{A} \times \frac{13[m_{\pi^+}]^2 f_\pi m_e G_F}{m_K^2} \times \frac{\alpha I(x_t)}{\pi \sin\theta_W^2}, \tag{9}$$

where $\mathcal{J}$ is the reduced Jarlskog invariant

$$\mathcal{J} = \text{Im}(V_{ts}^*V_{td}V_{ud}^*V_{us}) \simeq 3.1 \times 10^{-5}, \tag{10}$$

---

[1]The overall sign of a and b is not fixed by the hyperon nonleptonic decay (the relative sign between a and b is fixed to be negative). We use the sign motivated by the vacuum factorization of strong penguins [24, 26]. If the overall sign is opposite, it only affects the overall sign of C_S (and d_e^{equiv}) and not its absolute value.
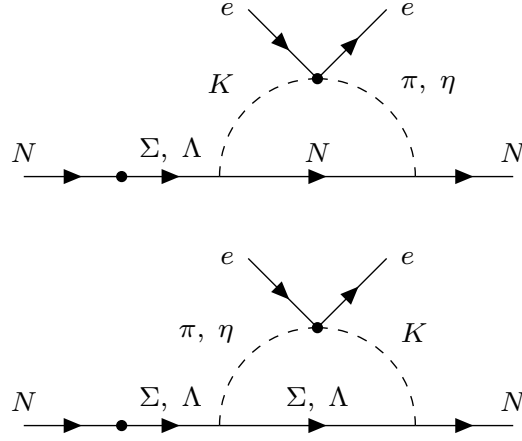
Figure 2: The baryon pole diagrams that contribute to C_S at the NLO level in the chiral limit. The diagrams with the nucleon-hyperon mixing on the right side give the same amount of contribution.

that carries about $\sim 6\%$ uncertainty. The overall scaling of this formula in the chiral limit and at large x_t is

$$G_F C_S \propto \mathcal{J} G_F^3 m_t^2 m_e m_s^{-1} \Lambda_{\text{hadr}}^2. \tag{11}$$

where Λ_{hadr} is the typical hadronic scale. Notice that this is far more singular behavior with m_q than that arising in the chiral-loop-induced expressions for d_n. Also notice that the K_S exchange dominates for any conventional parametrization of the CKM matrix, and the role of K_L exchange is to add small pieces of the amplitude that take $\text{Re}(V_{ud}V_{us}^*)\text{Im}(V_{ts}V_{td}^*)$, arising from K_S exchange, to the full $\mathcal{J}$. Substituting all the SM parameters, we obtain

$$C_S(\text{LO}) \simeq 5 \times 10^{-16}, \tag{12}$$

at the leading order in the chiral limit.

In order to estimate the accuracy of the above result, one could try to evaluate the Next-to-leading order (NLO) corrections in the expansion over small m_s. It turns out that the baryon pole diagrams, shown in Fig. 2, are the dominant correction in the chiral limit, as they scale as $m_K/\Lambda_{\text{hadr}} \sim \sqrt{m_s/\Lambda_{\text{hadr}}}$ relative to the leading order result. They are fully calculable without introducing any counterterms. With the heavy baryon chiral perturbation theory, we find that NLO corrections interfere constructively with LO, and give 30% correction for the proton, and 40% for the neutron, reqspectively. Combining LO and NLO, we arrive at our final result,

$$C_S(\text{LO} + \text{NLO}) \simeq 6.9 \times 10^{-16}, \quad \text{or} \quad d_e^{\text{equiv}} \simeq 1.0 \times 10^{-35} \, e \, \text{cm}. \tag{13}$$

From the size of the NLO corrections, we estimate the accuracy of our computation as $O(30\%)$. As stated before, this result is much larger than previously believed, and exceeds any contributions of d_e into d_e^{equiv} by at least four orders of magnitude. The enhancement of C_S at G_F^3 order compared to $\alpha^2 G_F^2$ can be roughly understood as $\alpha_W/\alpha^2 \sim O(10^3)$. We note that, although translating C_S to d_e^{equiv} depends on atoms/molecules that one considers, this dependence is mild and d_e^{equiv} is within the same ballpark if we instead consider, *e.g.*, Tl, YbF or HfF$^+$ [13].

3. Indirect constraints on muon EDM

As we saw above, the CKM contribution to d_e^{equiv} is still far below the current experimental sensitivity. This indicates that, once we find a non-zero result in those experiments, it definitely comes from new physics. In this section, we discuss one possible such new physics contribution to the paramagnetic EDMs, that is, the muon EDM:

$$\mathcal{L} = -\frac{i}{2} d_\mu \, \bar{\mu} \sigma_{\alpha\beta} F^{\alpha\beta} \gamma_5 \mu. \tag{14}$$

The latest interest in muons is fueled by the ongoing discrepancy between theoretical predictions and experimental measurements of the muon anomalous magnetic moment $g-2$ [16, 17]. This situation brings other observables that involve muons particularly interesting, and one such important quantity is the muon EDM d_μ (see *e.g.* [15] on the extended discussion on this point). At the moment, the storage ring EDM measurement at BNL sets the tightest bound on the muon EDM [19],

$$\left| d_\mu \right| < 1.8 \times 10^{-19} \, e \, \text{cm}, \tag{15}$$

but there are proposals on significantly improving this bound with dedicated storage ring type muon experiments [18, 20–22]. Given these upcoming efforts, it is important to reevaluate *indirect* bounds on muon EDM, especially given the significant progress in the precision of atomic/molecular EDM experiments in recent years. In the following, we focus on the paramagnetic EDM experiments, and quote only the final result for the diamagnetic EDM experiments. Readers interested in details of the latter calculation are referred to [27].

3.1 Electron EDM induced at three-loop

First, we evaluate the electron EDM induced by the heavy-lepton EDMs. The relevant diagrams are shown in Fig. 3 (and their permutations). Since there is a hierarchy in the mass, $m_l/m_L \ll 1$, where $l = e$ and $L = \mu, \tau$, we expand the diagrams with respect to m_l/m_L and p/m_L and evaluate only the leading terms, where p is the momentum of the external electron (which is of the same order as m_l due to the Dirac equation). In general, the amplitude contains two distinct Dirac structures that induce the EDM operator:

$$i\mathcal{M} = i\tilde{F}^{\mu\nu} \bar{e}(p) \left[S^{(1)} m_e \sigma_{\mu\nu} + S^{(2)} \left\{ \sigma_{\mu\nu}, \slashed{p} \right\} \right] e(p). \tag{16}$$

One can see that the second term is equivalent to the first one after using the equation of motion for electrons. Since we expand the integrals by m_e and p, $S^{(1)}$ and $S^{(2)}$ do not depend on these parameters, corresponding to the so-called scalar vacuum integral. $S^{(1)}$ and $S^{(2)}$ have a simple topology described by B_M in [28] and can be reduced to two master integrals by repeated use of integration by parts [29–33]. One of the master integrals is simply the product of three one-loop integrals, and the other is a three-loop integral corresponding to $\mathbf{E}(0, 0, x, x)$ in [33]. We use the `FIRE6` [34] package to perform the integration-by-parts reduction and use the analytical expressions of master integrals in [33]. Divergences and gauge dependencies in the two structures cancel out separately[2] and leave with us a finite result [35]:

$$d_l = \left(a^{(1)} + a^{(2)} \right) \frac{m_l}{m_L} \left(\frac{\alpha}{\pi} \right)^3 d_L, \tag{17}$$

---

[2]Each individual diagram contains divergences, and we exploit the dimensional regularization to tame them.
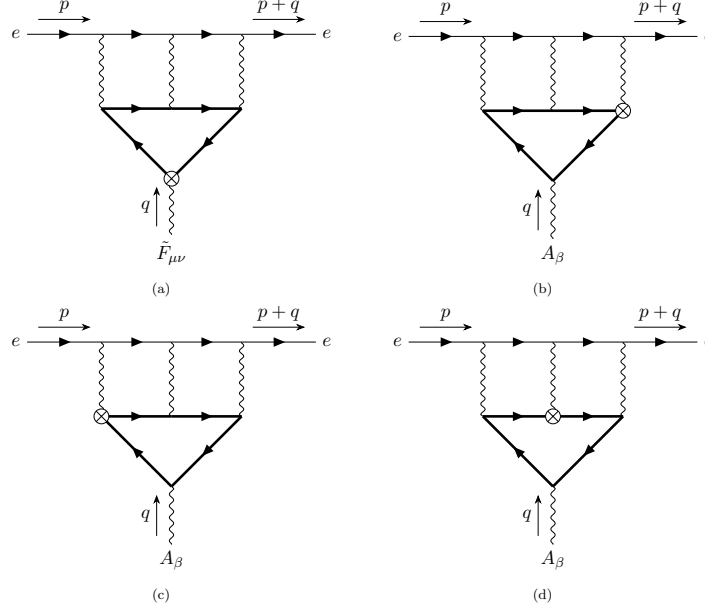
Figure 3: Three-loop QED diagrams for heavy lepton EDM contribution to electron EDM. The thin lines correspond to the electron, while the thick lines correspond to the heavy lepton. The crossed dots indicate the EDM operator insertions.

where

$$a^{(1)} = \frac{3}{2}\zeta(3) - \frac{19}{12}, \quad a^{(2)} = \frac{1}{2}\zeta(3) - \frac{1}{6}, \quad \zeta(3) \simeq 1.202. \tag{18}$$

The contribution from expansion in m_l/m_L is labeled by the upper index "(1)", and the contribution from expansion in p/m_L is labeled by the upper index "(2)".

Here is a comment. Grozin, Khriplovich, and Rudenko in [36] showed, for the first time, that heavy leptons (muon and tau lepton) induce an electron EDM at the three-loop order, and put indirect constraints on heavy-lepton EDMs based on electron EDM experiments. Comparing with [36], we see that their result corresponds to our $a^{(1)}$, while the contribution from $a^{(2)}$ is not included. This means that they expanded the amplitude in m_e/m_τ but overlooked the expansion in p/m_τ. Our calculation shows that both contribute to the electron EDM at the same order. Numerically our result is $\sim 40\%$ larger than [36]. As a double-check of our procedure, we reevaluated the leading order contribution to the electron $g - 2$ induced by a muon loop (without the EDM operator insertion). This contribution to the electron $g - 2$ has been extensively studied by many groups and is better known [37, 38]. Our procedure reproduces the known result correctly, and both expansions in m_e/m_μ and in p/m_μ need to be included to get the correct result.

3.2 Semi-leptonic CP-odd operator

We next evaluate C_S induced by the muon EDM. Once we go below the muon mass scale, in addition to the electron EDM, the muon EDM induces CP-odd nonlinear electromagnetic interactions. The left diagram of Fig. 4 is an example of such a diagram. We notice that photon
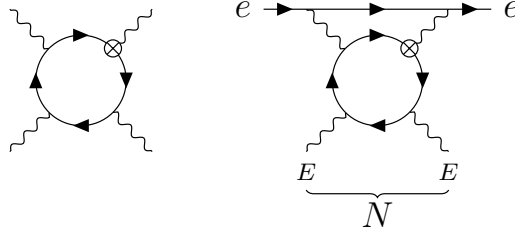
Figure 4: A representative light-by-light scattering diagram with d_μ insertion (indicated by the crossed dot) giving rise to $E^3 B$ interaction. The closed solid line corresponds to the off-shell muon. When E^2 is sourced by the nucleus and EB is connected to the electron, as shown on the right, it induces an equivalent C_S operator.

momenta entering the muon loop are small compared to the muon mass m_μ. Indeed, in a large nucleus with $q_\gamma^{\max} \sim R_N^{-1} \sim 30\,\text{MeV}$, one can keep only the lowest dimension operators, and omit the operators that involve derivatives acting on the electric $\mathbf{E}$ and magnetic $\mathbf{B}$ fields. To linear order in d_μ, we directly compute the corresponding electromagnetic operators, similar to the dimension eight terms in the Euler-Heisenberg Lagrangian:

$$\mathcal{L} = -e^4 (\tilde{F}_{\alpha\beta} F^{\alpha\beta})(F_{\gamma\delta} F^{\gamma\delta}) \times \frac{d_\mu/e}{96\pi^2 m_\mu^3} = -\frac{d_\mu/e}{12\pi^2 m_\mu^3} e^4 (\mathbf{E} \cdot \mathbf{E})(\mathbf{E} \cdot \mathbf{B}) + \cdots . \tag{19}$$

where we ignore the $O(B^3)$ interaction in the last equality that is subdominant due to no Z enhancement.

The $E^3 B$ term generates the semileptonic CP-odd operator via the right diagram of Fig. 4. The two electric field lines are sourced by the nucleus, while the photon loop attached to the electron line generates the $m_e \bar{e} i \gamma_5 e$ structure. Being concentrated inside and near the nucleus, $\mathbf{E}^2$ can be considered *equivalent* to the delta-functional contribution:

$$e^2 (\mathbf{E}^2)_{\text{nucl}} \rightarrow \delta(\mathbf{r}) \times \frac{24\pi (Z\alpha)^2}{5 R_N}, \tag{20}$$

where we assume a constant density charge distribution. Since the nucleon number density operator $\bar{N}N$ is also localized at the position of the nucleus, one can think of these two operators as equivalent. The photon loop is enhanced by a logarithm $\log(\Lambda/m_e)$, and we evaluate it to leading logarithmic accuracy by taking $\Lambda = m_\mu$.[3] Putting the results of the loop calculation together with (20), we arrive at the following prediction for the *equivalent* C_S value:

$$\frac{G_F}{\sqrt{2}} C_S^{\text{equiv}} = \kappa \frac{4 Z^2 \alpha^4}{\pi A} \times \frac{m_e (d_\mu/e)}{m_\mu^3 R_N} \times \log \left(\frac{m_\mu}{m_e} \right), \tag{21}$$

where the fudge factor κ accounts for the different distributions of $\mathbf{E}^2$ and $\bar{N}N$. Solving the Dirac equation near the nucleus for the outside $s_{1/2}$ and $p_{1/2}$ electron wave functions and finding a ratio of the matrix elements for these two distributions result in $\kappa \simeq 0.66$. As one can see, C_S^{equiv} scales as $Z^2 A^{-1} R_N^{-1} \propto Z^{2/3}$, which is the sign of coherent enhancement. Numerically we obtain

$$C_S^{\text{equiv}} = 3.1 \times 10^{-10} \left(\frac{d_\mu}{10^{-20}\, e\,\text{cm}} \right) . \tag{22}$$

---

[3]In practice, this cutoff will be supplied by the non-local nature of the muon loop in the right diagram of Fig. 1.

8

3.3 Constraints on muon EDM

By combining the results of d_e and C_S obtained above, we derive an indirect constraint on muon EDM from the paramagnetic EDM experiment [27, 35]:

$$|d_\mu| < 1.7 \times 10^{-20} \, e \, \text{cm}. \tag{23}$$

We observe that d_e and C_S interfere constructively, and the C_S contribution is larger by a factor of $\simeq 3$. We believe that Eq. (22) is accurate within $\sim$ 15–20% with uncertainties associated with the modeling of $\mathbf{E}(r)$ and the logarithmic approximation for the photon loop integral.

Although we have not discussed, the CP-odd photon operator E^3B induces the Schiff moment probed by diamagnetic EDM experiments as well. In particular, from ^{199}Hg [1], we obtain the upper bound on the muon EDM as

$$|d_\mu| < 6.4 \times 10^{-20} \, e \, \text{cm}. \tag{24}$$

Although this is weaker than the paramagnetic EDM experiments, this is stronger than the direct constraint by the BNL experiment. Given that the paramagnetic and diamagnetic systems are completely different, this result strengthens the robustness of our indirect limits on the muon EDM.

Finally, we can apply our result to the tau EDM by simply replacing m_μ by m_τ. We thus update the constraint on the tau EDM:

$$|d_\tau| < 1.1 \times 10^{-18} e \, \text{cm} \quad (90\% \text{C.L.}). \tag{25}$$

In the case of tau EDM, the C_S operator is suppressed since it scales as $C_S \propto m_L^{-3}$, and d_e induced by d_τ dominates. While there is only a small change from the previous work on the three-loop computation side (from $S^{(2)}$), the accuracy of the paramagnetic experiments has improved by two orders of magnitude since the time [36] was published. As a result, the indirect constraint on d_τ is now tighter than the one from $e^+e^- \to \tau^+\tau^-$ by the Belle experiment [39]. The Belle-II experiment plans to measure d_τ, again by $e^+e^- \to \tau^+\tau^-$, with an accuracy of $|\text{Re}\, d_\tau|, |\text{Im}\, d_\tau| < 10^{-18}$–$10^{-19} \, e$ cm [40]. Therefore Eq. (25) provides an important benchmark for the Belle-II experiment. We note that the studies of the tau-lepton electromagnetic form factors will greatly benefit from the proposed addition of the longitudinal polarization to the electron beam [41], and several orders of magnitude improvements are possible [42, 43].

4. Conclusion

In this paper, we have reviewed recent theoretical developments in the field of the EDM. In particular, we have discussed two CP violating contributions to the paramagnetic EDM experiments; Standard Model CKM phase and the muon EDM.

In the former case, we have found that a Kaon-exchange contribution, combining weak non-leptonic transition with the semileptonic electroweak penguin, is larger by three orders of magnitude than the previous estimation. Numerically we have obtained

$$d_e^{\text{equiv}} = 1.0 \times 10^{-35} \, e \, \text{cm}. \tag{26}$$

This contribution is rather precisely calculable with the chiral perturbation theory. Indeed, we have evaluated the NLO correction in the chiral limit, which allows us to estimate the precision of our calculation as $O(30\%)$. Although the result is still small, it is not unthinkable that the progress in sensitivity to the paramagnetic EDMs may reach the level of d_e^{equiv} in the future. Indeed, some novel proposals [8] envision at detecting $d_e \sim O(10^{-35}\text{–}10^{-37})\,e\,\text{cm}$.

Then we have evaluated the electron EDM d_e and the semileptonic CP-odd operator C_S induced from the muon EDM. We have computed a three-loop contribution from d_μ to d_e that was overlooked in the previous literature. Moreover, we have found that muon-loop-induced E^3B effective interaction leads to C_S enhanced by a coherent factor $Z^{2/3}$. By combining those results, we obtain an upper bound on the muon EDM from the paramagnetic EDM experiment as

$$\left|d_\mu\right| < 1.7 \times 10^{-20}\,e\,\text{cm}. \tag{27}$$

Although we have not explained it in detail, the E^3B operator also induces the Schiff moment S_N probed by the diamagnetic EDM experiments. From the mercury EDM experiment, we obtain

$$\left|d_\mu\right| < 6.4 \times 10^{-20}\,e\,\text{cm}. \tag{28}$$

These are already stronger than the direct bound at BNL (15). Eq. (27) provides a new benchmark that future dedicated muon EDM experiments would have to overtake. We also notice that since both ^{199}Hg and ThO EDM results give an improvement, it is highly unlikely that a fine-tuned choice of d_e and hadronic CP-violation would lead to the relaxation of indirect bounds on d_μ.

Finally, we have updated the limit on the τ-lepton EDM d_τ derived in [36]. In this case, the electron EDM plays the dominant role since $d_e \propto m_\tau^{-1}$ while $S_N, C_S \propto m_\tau^{-3}$ up to logarithm. From the ThO molecule, we obtain

$$|d_\tau| < 1.6 \times 10^{-18}\,e\,\text{cm}. \tag{29}$$

This surpasses the constraint from the Belle experiment [39].

Acknowledgement

References

[1] B. Graner, Y. Chen, E.G. Lindahl and B.R. Heckel, *Reduced Limit on the Permanent Electric Dipole Moment of Hg199*, *Phys. Rev. Lett.* **116** (2016) 161601 [1601.04339].

[2] W.B. Cairncross, D.N. Gresh, M. Grau, K.C. Cossel, T.S. Roussy, Y. Ni et al., *Precision Measurement of the Electron's Electric Dipole Moment Using Trapped Molecular Ions*, *Phys. Rev. Lett.* **119** (2017) 153001 [1704.07928].

[3] ACME collaboration, *Improved limit on the electric dipole moment of the electron*, *Nature* **562** (2018) 355.

[4] C. Abel et al., *Measurement of the Permanent Electric Dipole Moment of the Neutron*, *Phys. Rev. Lett.* **124** (2020) 081803 [`2001.11966`].

[5] J.S.M. Ginges and V.V. Flambaum, *Violations of fundamental symmetries in atoms and tests of unification theories of elementary particles*, *Phys. Rept.* **397** (2004) 63 [`physics/0309054`].

[6] M. Pospelov and A. Ritz, *Electric dipole moments as probes of new physics*, *Annals Phys.* **318** (2005) 119 [`hep-ph/0504231`].

[7] J. Engel, M.J. Ramsey-Musolf and U. van Kolck, *Electric Dipole Moments of Nucleons, Nuclei, and Atoms: The Standard Model and Beyond*, *Prog. Part. Nucl. Phys.* **71** (2013) 21 [`1303.2371`].

[8] A.C. Vutha, M. Horbatsch and E.A. Hessels, *Oriented polar molecules in a solid inert-gas matrix: a proposed method for measuring the electric dipole moment of the electron*, *Atoms* **6** (2018) 3 [`1710.08785`].

[9] A.C. Vutha, M. Horbatsch and E.A. Hessels, *Orientation-dependent hyperfine structure of polar molecules in a rare-gas matrix: A scheme for measuring the electron electric dipole moment*, *Phys. Rev. A* **98** (2018) 032513 [`1806.06774`].

[10] T. Fleig and D. DeMille, *Theoretical aspects of radium-containing molecules amenable to assembly from laser-cooled atoms for new physics searches*, *New J. Phys.* **23** (2021) 113039 [`2108.02809`].

[11] M. Kobayashi and T. Maskawa, *CP Violation in the Renormalizable Theory of Weak Interaction*, *Prog. Theor. Phys.* **49** (1973) 652.

[12] Y. Yamaguchi and N. Yamanaka, *Large long-distance contributions to the electric dipole moments of charged leptons in the standard model*, *Phys. Rev. Lett.* **125** (2020) 241802 [`2003.08195`].

[13] M. Pospelov and A. Ritz, *CKM benchmarks for electron electric dipole moment experiments*, *Phys. Rev. D* **89** (2014) 056006 [`1311.5537`].

[14] Y. Ema, T. Gao and M. Pospelov, *Standard Model prediction for paramagnetic EDMs*, `2202.10524`.

[15] A. Crivellin, M. Hoferichter and P. Schmidt-Wellenburg, *Combined explanations of $(g-2)_{\mu,e}$ and implications for a large muon EDM*, *Phys. Rev. D* **98** (2018) 113002 [`1807.11484`].

[16] T. Aoyama et al., *The anomalous magnetic moment of the muon in the Standard Model*, *Phys. Rept.* **887** (2020) 1 [`2006.04822`].

[17] MUON G-2 collaboration, *Measurement of the Positive Muon Anomalous Magnetic Moment to 0.46 ppm*, *Phys. Rev. Lett.* **126** (2021) 141801 [2104.03281].

[18] Y.K. Semertzidis et al., *Sensitive search for a permanent muon electric dipole moment*, in *KEK International Workshop on High Intensity Muon Sources (HIMUS 99)*, pp. 81–96, 12, 1999, DOI [hep-ph/0012087].

[19] MUON (G-2) collaboration, *An Improved Limit on the Muon Electric Dipole Moment*, *Phys. Rev. D* **80** (2009) 052008 [0811.1207].

[20] H. Iinuma, H. Nakayama, K. Oide, K.-i. Sasaki, N. Saito, T. Mibe et al., *Three-dimensional spiral injection scheme for the g-2/EDM experiment at J-PARC*, *Nucl. Instrum. Meth. A* **832** (2016) 51.

[21] M. Abe et al., *A New Approach for Measuring the Muon Anomalous Magnetic Moment and Electric Dipole Moment*, *PTEP* **2019** (2019) 053C02 [1901.03047].

[22] A. Adelmann et al., *Search for a muon EDM using the frozen-spin technique*, 2102.08838.

[23] T. Inami and C.S. Lim, *Effects of Superheavy Quarks and Leptons in Low-Energy Weak Processes k(L) —> mu anti-mu, K+ —> pi+ Neutrino anti-neutrino and K0 <—> anti-K0*, *Prog. Theor. Phys.* **65** (1981) 297.

[24] M.A. Shifman, A.I. Vainshtein and V.I. Zakharov, *Light Quarks and the Origin of the Delta I = 1/2 Rule in the Nonleptonic Decays of Strange Particles*, *Nucl. Phys. B* **120** (1977) 316.

[25] J. Bijnens, H. Sonoda and M.B. Wise, *On the Validity of Chiral Perturbation Theory for Weak Hyperon Decays*, *Nucl. Phys. B* **261** (1985) 185.

[26] J. Tandean and G. Valencia, *CP violation in hyperon nonleptonic decays within the standard model*, *Phys. Rev. D* **67** (2003) 056001 [hep-ph/0211165].

[27] Y. Ema, T. Gao and M. Pospelov, *Improved Indirect Limits on Muon Electric Dipole Moment*, *Phys. Rev. Lett.* **128** (2022) 131803 [2108.05398].

[28] D.J. Broadhurst, *Three loop on-shell charge renormalization without integration: Lambda-MS (QED) to four loops*, *Z. Phys. C* **54** (1992) 599.

[29] L.V. Avdeev, *Recurrence relations for three loop prototypes of bubble diagrams with a mass*, *Comput. Phys. Commun.* **98** (1996) 15 [hep-ph/9512442].

[30] M. Steinhauser, *MATAD: A Program package for the computation of MAssive TADpoles*, *Comput. Phys. Commun.* **134** (2001) 335 [hep-ph/0009029].

[31] K.G. Chetyrkin and F.V. Tkachov, *Integration by Parts: The Algorithm to Calculate beta Functions in 4 Loops*, *Nucl. Phys. B* **192** (1981) 159.

[32] F.V. Tkachov, *A Theorem on Analytical Calculability of Four Loop Renormalization Group Functions*, *Phys. Lett. B* **100** (1981) 65.

[33] S.P. Martin and D.G. Robertson, *Evaluation of the general 3-loop vacuum Feynman integral*, *Phys. Rev. D* **95** (2017) 016008 [1610.07720].

[34] A.V. Smirnov and F.S. Chuharev, *FIRE6: Feynman Integral REduction with Modular Arithmetic*, *Comput. Phys. Commun.* **247** (2020) 106877 [1901.07808].

[35] Y. Ema, T. Gao and M. Pospelov, *Reevaluation of heavy-fermion-induced electron EDM at three loops*, *Phys. Lett. B* **835** (2022) 137496 [2207.01679].

[36] A.G. Grozin, I.B. Khriplovich and A.S. Rudenko, *Electric dipole moments, from e to tau*, *Phys. Atom. Nucl.* **72** (2009) 1203 [0811.1641].

[37] S. Laporta and E. Remiddi, *The Analytical value of the electron light-light graphs contribution to the muon (g-2) in QED*, *Phys. Lett. B* **301** (1993) 440.

[38] J.H. Kuhn, A.I. Onishchenko, A.A. Pivovarov and O.L. Veretin, *Heavy mass expansion, light by light scattering and the anomalous magnetic moment of the muon*, *Phys. Rev. D* **68** (2003) 033018 [hep-ph/0301151].

[39] BELLE collaboration, *Search for the electric dipole moment of the tau lepton*, *Phys. Lett. B* **551** (2003) 16 [hep-ex/0210066].

[40] BELLE-II collaboration, *The Belle II Physics Book*, *PTEP* **2019** (2019) 123C01 [1808.10567].

[41] J.M. Roney, *Electroweak Physics with Polarized Beams at SuperKEKB Upgrade*, *PoS* **LeptonPhoton2019** (2019) 109 [1907.03503].

[42] J. Bernabeu, G.A. Gonzalez-Sprinberg, J. Papavassiliou and J. Vidal, *Tau anomalous magnetic moment form-factor at super B/flavor factories*, *Nucl. Phys. B* **790** (2008) 160 [0707.2496].

[43] A. Crivellin, M. Hoferichter and J.M. Roney, *Towards testing the magnetic moment of the tau at one part per million*, 2111.10378.

[44] J. Ellis, *TikZ-Feynman: Feynman diagrams with TikZ*, *Comput. Phys. Commun.* **210** (2017) 103 [1601.05437].